WIRELINE LOG AND BOREHOLE IMAGE INTERPRETATION FOR FORGE WELL 58-32, BEAVER COUNTY, UTAH, AND INTEGRATION WITH CORE DATA

by David A. Handwerger[1] and John D. McLennan[2]

[1]Statistical Petrophysics, LLC, and Energy and Geosciences Institute, Salt Lake City, Utah
[2]Department of Chemical Engineering, University of Utah, Salt Lake City, Utah

Link to supplemental data download: https://ugspub.nr.utah.gov/publications/misc_pubs/mp-169/mp-169-m.zip

Appendices 1 & 2

Figures 4–7

Miscellaneous Publication 169-M
Utah Geological Survey
a division of
UTAH DEPARTMENT OF NATURAL RESOURCES

This paper is part of *Geothermal Characteristics of the Roosevelt Hot Springs System and Adjacent FORGE EGS Site, Milford, Utah*. https://doi.org/10.34191/MP-169

Bibliographic citation:

Handwerger, D.A., and McLennan, J.D., 2019, Wireline log and borehole image interpretation for FORGE well 58-32, Beaver County, Utah, and integration with core data, *in* Allis, R., and Moore, J.N., editors, Geothermal characteristics of the Roosevelt Hot Springs system and adjacent FORGE EGS site, Milford, Utah: Utah Geological Survey Miscellaneous Publication 169-M, 7 p., 2 appendices, supplemental data, https://doi.org/10.34191/MP-169-M.

WIRELINE LOG AND BOREHOLE IMAGE INTERPRETATION FOR FORGE WELL 58-32, BEAVER COUNTY, UTAH, AND INTEGRATION WITH CORE DATA

by David A. Handwerger and John D. McLennan

ABSTRACT

A series of wireline logs were collected in the Frontier Observatory for Research in Geothermal Energy (FORGE) well 58-32, which is located just west of the Mineral Mountains, northeast of Milford, Utah, to characterize the mechanical properties and stress framework of the rock and the fracture network. A baseline logging phase was carried out over the majority of the borehole (below surface casing) upon completion of drilling and coring operations, and included Triple Combo, Dipole Sonic (DSI) and Formation Micro-Imager (FMI) logs. A second logging phase was conducted after openhole injection and microhydraulic fracturing had been carried out in the bottom, uncased section of the wellbore (~150 ft). This second logging suite consisted of a repeat FMI run over the lowermost ~110 ft to observe the changes in the fractures following the injection.

Many drilling-induced natural fractures were observed, having an average azimuth of 219 degrees, but most common direction of around 206 degrees (N26E). This azimuth typically corresponds to the direction of maximum horizontal stress. Minor borehole breakouts, also identifiable from the FMI images and which typically occur in the direction of minimum horizontal stress, had an average azimuth of 297 degrees (NW-SE), as would be expected given the interpreted orientation of the orthogonal stress from the induced fractures. The breakouts suggest an average azimuth of the maximum horizontal stress of N27E (i.e., minimum horizontal stress of N53W).

Additional continuous mechanical properties were calculated from the P- and S-wave velocities measured by a dipole sonic log, and bulk density from conventional triple combo measurements. The dipole sonic data were calibrated to triaxial compression tests on samples taken from the two cored sections in the well. These procedures enabled conversion of the dynamically-derived log predictions to static-equivalent parameters required for true subsurface mechanical property calculations. Calibration to core also allowed for calculation of a continuous Biot's parameter over the logged interval. This parameter is useful for estimation of the in situ stresses. From the calibrated mechanical properties, independent assessment of the formation pore pressure, and a calculation of Biot's poroelastic parameter, the principal stress magnitudes were estimated over the majority of the borehole.

New methods were employed to interpret changes in the subsurface fracture state because this project was unique in recording two FMI logs at different times. The before and after images were carefully realigned and then digitally subtracted in order to highlight any changes associated with a moderately aggressive injection program. This comparison enabled identifying newly induced fractures as well as widening and lengthening of previously observed natural fractures. Additionally, non-planar vertical fractures, perturbed in response to small-scale textural heterogeneities in the granite, were observed, suggesting localized stress concentrations and associated complexities (relative to strictly planar features) in the induced fractures.

INTRODUCTION

Wireline logging is an important means to gather data on the geology and material properties of the subsurface. Logging is conducted by lowering a series of instruments down a borehole and recording the physical properties of the rock as the instruments are pulled back up the hole at a set speed, typically around 1800 ft/hr. Logs record multiple physical responses in the rock and are sensitive to mineralogy, porosity, fluid saturation, fluid type, mechanical properties and fracturing. Logging data are recorded continuously at discrete spacing along the logged section and have the advantage over seismic data in that they are higher resolution (less vertically smoothed) and less correlated to each other. This allows for easier interpretation and more unique solutions to various iterative models commonly employed to determine rock properties. Although acoustic logs record at higher frequency, they do not provide 3D subsurface data like seismic imaging does.

Data collected during two phases of logging conducted after the 58-32 (Figure 1) well was drilled were analyzed. Logging phase 1 (run 1) was conducted from the base of the surface casing at ~2172 ft logging depth to total depth (TD). Logging phase 2 (run 2) was conducted after production casing was run to 7374.9 ft measured depth (MD). Plugback TD in this hole is 7525 ft MD, leaving approximately 150 ft of open hole. This second logging campaign followed a series of injection tests in the barefoot region of the hole from the base of the production casing at ~7386 ft logging depth to TD. The production casing was run before the injection testing. The first logging phase consisted of a Triple Combo run, followed by a Dipole Sonic Imager (DSI) – Formation Micro-Imager (FMI) run. The second phase consisted of just a DSI – FMI run to canvas changes in the openhole section after the injection testing. The injection involved multiple cycles above fracturing pressure including two Diagnostic Fracture Injection Tests (DFITs), one step rate test (SRT) and a low rate (~9 barrels per minute, BPM, 2 L/s) injection cycle with 200 mesh $CaCO_3$ proppant, as well as a number of low-rate injection cycles for stress measurement (see, for example, Forbes et al., 2019).

The triple combo is a combination logging tool that includes three primary measurement sondes used for subsequent interpretation: gamma ray (natural radioactivity of the rock), electrical resistivity (or reciprocally, the electrical conductivity), and lithodensity (Schlumberger, 1989). The triple combo contains sensors which record data through physical contact to the borehole wall. The lithodensity measurements provide three measurements: the bulk density, the neutron porosity (essentially the hydrogen abundance, interpreted under the assumption that the amount of hydrogen in the formation reflects the amount of water and/or hydrocarbon [Schlumberger, 1989; Krygowski, 2003]), and the photoelectric cross section of the rock matrix, which is a function of constituent atomic numbers (Krygowski, 2003). The first two calculated values, the density and neutron

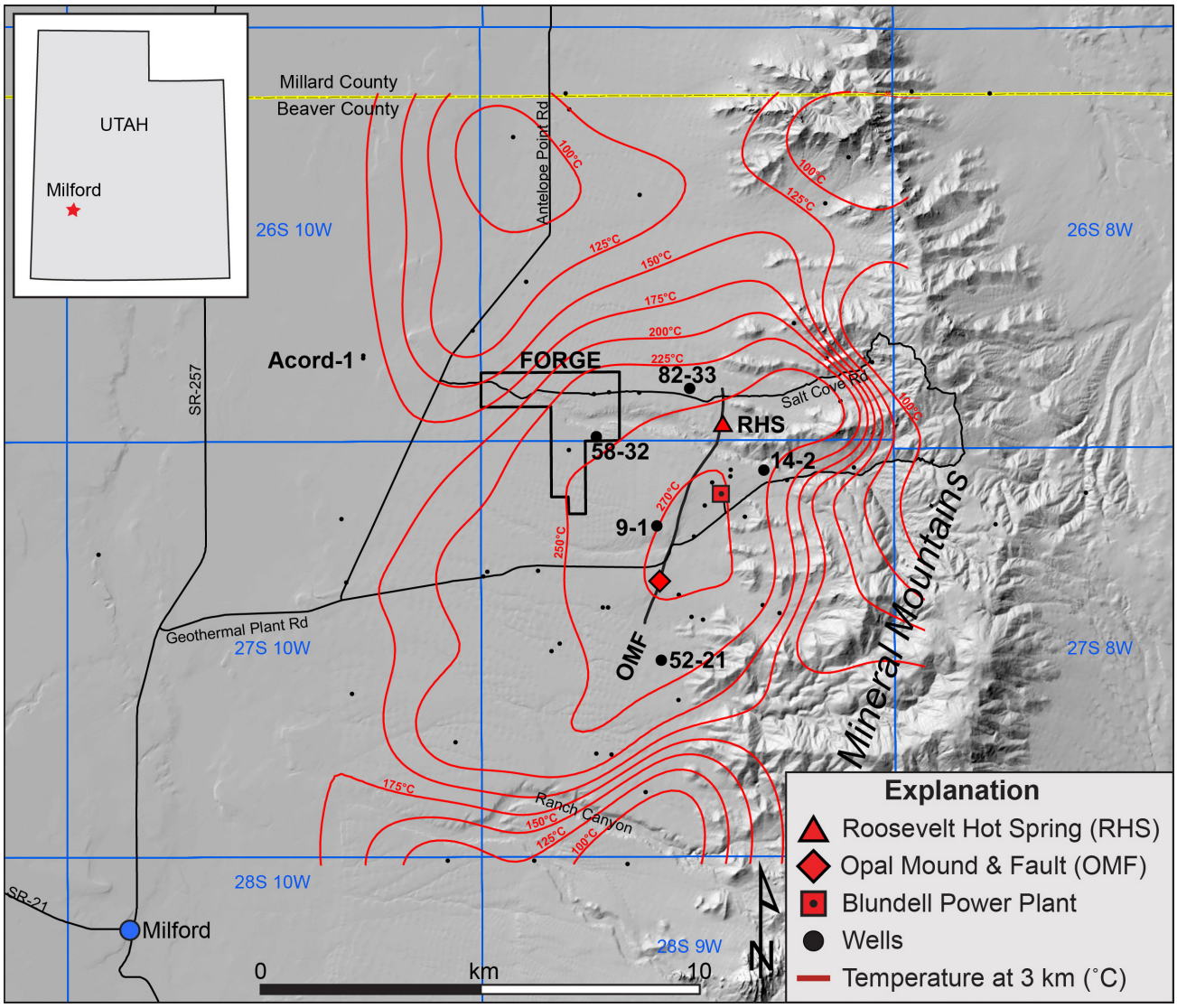

Figure 1. *Map showing the location of the FORGE 58-32 and nearby historical wells. Wells having data plotted in Appendix 2 are labeled. Other well locations shown are for historical thermal gradient wells. The isotherm contours displayed are from Allis et al. (2019).*

porosity, use fundamental measurements as proxies for formation porosity, liquid saturation, and fluid type. The gamma-ray count is a proxy for lithology (potassium, uranium, and thorium content; Schlumberger, 1989; Krygowski, 2003).

The DSI-FMI is a combination of two other logging tools. These were run concurrently but separately from the triple combo. A separate logging was required since these are run eccentrically in the borehole. The DSI log consists of a sonic source-receiver package to measure the velocity of acoustic waves in the rock, often viewed as a porosity proxy, but also fundamental for calculating geomechanical properties. The FMI records 192 short-spaced electrical resistivity measurements from a series of pads that contact about 80% of the borehole wall at any depth. Through these high-resolution measurements, an FMI survey returns an image of the borehole wall's features, particularly fractures (which are liquid filled and therefore much more conductive than the rock matrix) and pores. FMI images have millimeter-scale resolution (Schlumberger, 1989).

FRACTURE INTERPRETATION

Log analysis consisted of several steps. The first was interpretation and orientation of various fracture types and other planar features from the two FMI runs. An initial interpretation was provided by the logging contractor. We supplemented that interpretation, focusing on quality-controlling the initial interpretation and then adding additional important features that were overlooked. Numerous such features (tensile-induced fractures, breakouts, partially conductive fractures, conductive fractures, petal fractures, bedding planes, faults, etc.) were added to the initial interpretation, with particular attention to the lower 1000 ft of section, considered to be the thermal reservoir with in situ temperature exceeding 175°C. In the lowermost 1000 ft of the baseline FMI survey, only missed tensile-induced fractures, breakouts, and obvious bed boundaries were added to the fracture inventory developed by the logging contractor. Appendix 1 shows the baseline FMI image log with both the initial interpretation (left half) and the refined interpretation (right half). Figure 2 shows the distribution of tensile-induced (drilling induced) fractures from a merged set of the initial and refined interpretations. Figure 3 shows the merged breakouts. These data are important because tensile-induced fractures indicate the direction of the maximum horizontal stress and the borehole breakouts indicate the direction of the minimum horizontal stress. Each rose diagram shows the dip azimuth, with the average (solid arrow) and mode (dashed arrow) of the azimuths indicated. The drilling-induced fractures are oriented with a median azimuth of ~26° (NNE-SSW), and the breakouts are oriented with an average azimuth of ~297 degrees (NW-SE). Since some apparent breakouts were hard to conclusively identify as breakouts rather than induced fractures, feature orientation was used as a consideration for their interpretation in a number of cases.

The main interest in running an FMI log before and after the hydraulic fracturing in the barefoot section of the hole was to compare the two images and look for changes. We did this by taking the two static-processed FMI images and digitally subtracting one from the other. The static-processed images display the resistivity data with a color palette partitioned by the range of microresistivity values over the entire vertical recorded section, as opposed to a dynamically-processed image where the color palette is partitioned by microresistivity values within a small sliding window. Image subtraction required the use of the constant baseline imaging provided by the static processing.

To subtract the images as precisely as possible, they had to be depth-shifted relative to each other by refining the alignment of obviously identical features. Typically, each logging tool string contains a gamma-ray tool that provides a high-fidelity indication of lithology. As such, it is commonly used to depth-align the measurements from separate logging runs. In this case, the precision of this initial alignment of the two runs was not sufficient for the task of image subtraction. A refined, more precise alignment was made using like features in the FMI. Figure 4 shows the realigned and subtracted image logs.

Features present in the run-2 image that are not present in the run-1 image appear as black in the subtracted image, and features present in run 1, but not run 2 appear as white. While we were able to adjust the depths of the images to improve alignment, our software was unable to adjust the azimuth (left-right) alignment, so there are some thin wispy features in the subtracted image that result from very slight azimuthal misalignment. The background "zero" color signifying similar features in both images is the orange hue that makes up most of the area. Examples of vertical (induced) fractures that appear in run 2, but not run 1 can be found at 7452 ft, 7461.5 ft, 7468.5 ft MD. One can also note a widening of a fracture at 7509 ft and a long fracture from 7526 to 7532 ft, among others. All of these fractures are oriented approximately S-SW. A series of non-vertical fractures appears from 7537.5 to 7542.5 ft, predominantly dipping towards the east.

During propagation, a hydraulic fracture that is growing in a nominally homogeneous medium will minimize the expenditure of energy by aligning perpendicular to the least local stress. Around well 58-32, the in situ stress measurements have suggested that this minimum stress will likely act horizontally. Knowing the azimuth of that minimum horizontal principal stress allows for approximating the direction that hydraulic fractures will grow. Although this directionality can be locally varied by natural

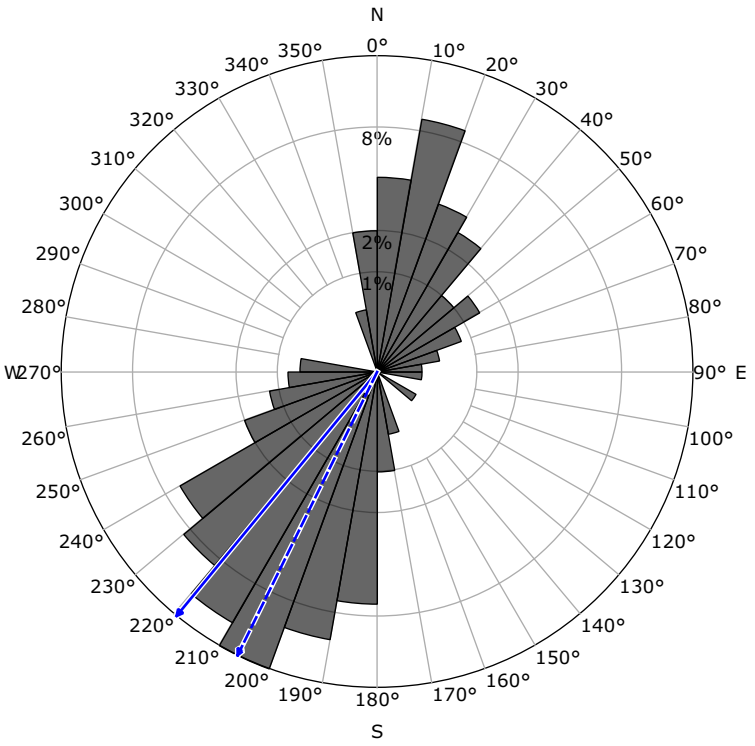

Figure 2. *Orientation of the tensile-induced natural fractures over the logged interval of the 58-32 well, including both those interpreted by the logging contractor and those that we added. Given that tensile-induced fractures are vertical to near-vertical, they do not appear as the sinusoids more gently dipping planes would, but as vertical traces on opposite sides of the borehole. To ensure that we did not identify the same feature twice, we only "picked" the most prominent trace. The traces, as identified, are shown rather than showing a reflection of one side to the other. This explains the lack of symmetry in the stereonet plot. We interpret the most common orientation as the direction of maximum horizontal stress.*

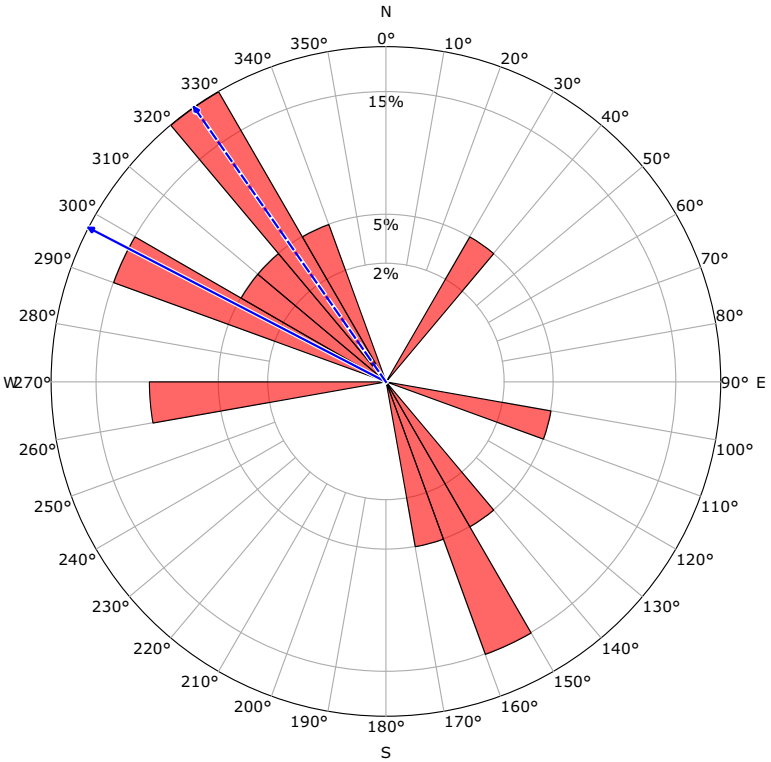

Figure 3. *Orientation of the borehole breakouts in the 58-32 well, following the same plotting guidelines as for the tensile-induced fractures in Figure 2. There were many fewer borehole breakouts than tensile-induced fractures, and they are much harder to interpret, accounting for the scatter in the data. The average orientation is approximately orthogonal to the tensile-induced fractures, suggesting this as the direction of minimum horizontal stress.*

discontinuities such as fractures, the propagation trend will be maintained at a large scale. If the propagation direction of hydraulically induced fractures in the vicinity of well 58-32 can be determined (that is, a vertical fracture, propagating in a plane containing the vertical stress and the maximum horizontal principal stress—perpendicular to the minimum horizontal principal stress), horizontal wellbores drilled in the minimum principal horizontal stress direction can ideally be stimulated multiple times to create a multitude of borehole-transverse horizontal fractures. As has been indicated, drilling-induced tensile fractures, tensile fractures created by hydraulic fracturing, and breakouts are all indicators of the directions of the horizontal stresses in the project area. In addition, if hydraulic shearing is a mechanism for growing a connective fracture network, then determination of the strike and dip of the most critically stressed, pre-existing fractures depends on the complete principal stress tensor (magnitude and direction of the three principal stresses as mentioned above).

GEOMECHANICAL INTERPRETATION

Using the dipole sonic data, we calculated the elastic parameters of the rock and then estimated the stresses (Figure 5). We calculated the dynamic Young's Modulus, E_D, dynamic Poisson's Ratio, ν_D, and dynamic Bulk Modulus, K_D (not shown). The dynamic values of Young's modulus and Poisson's ratio were calculated from wave velocities following standard protocols (Jaeger et al., 2009). The vertical stress was calculated by integrating the bulk density over the entire true vertical depth. This calculation required extrapolating the bulk density from the first logging measurement to an estimated surface value.

Two sets of triaxial tests were conducted from samples collected in both cores that were acquired in the well. With measurements at different confining pressures, cohesion and the angle of internal friction were determined. Static values of Young's Modulus, E_S, Poisson's Ratio, ν_S, and Bulk Modulus, K_S, were determined from these tests following accepted practices (Ulusay and Hudson, 2007). Those data are shown in Figure 5 in comparison to the log-based calculations (note, the core depths have been adjusted to align with log depth; see below). The core data represent static properties. The dynamic Young's Modulus was calibrated to the core data to provide a continuous static Young's Modulus curve. Since Poisson's ratios from the core generally align with the log-calculated values at and near the core point, Poisson's ratio was not further calibrated. This is accepted industry practice—correcting the dynamic moduli using the static data but not adjusting Poisson's ratio. The logging-based values of Poisson's ratio were used as-is for estimating the horizontal stresses.

Biot's poroelastic parameter was calculated using a constant bulk modulus of quartz of 5.3×10^6 psi, derived from published data on manufactured quartz (Crystran, 2018), and from there the minimum and maximum horizontal stresses were calculated. According to a variation of Eaton's model, stresses were estimated using a poro-uniaxial strain model; i.e., with the assumption of zero far-field lateral strain (Eaton, 1969). Biot's poroelastic parameter, α, is estimated in a conventional manner as one minus the ratio of the grain or solid compressibility to the static compressibility of the bulk medium (Detournay and Cheng, 1993). The grain compressibility was approximated as the reciprocal of the bulk modulus of quartz. Biot's poroelastic parameter was initially calculated using the dynamic bulk modulus, and then recalculated with a "calibrated" static bulk modulus derived from Poisson's ratio and the logging values that have been calibrated with the laboratory measurements. Figure 5 shows the minimum and maximum horizontal stresses (solid green and red curves in the stresses column) for the uncalibrated log data, and the minimum horizontal stress (dashed green curve) for the calibrated logging data. Both maximum and minimum horizontal stresses were further adjusted to match the stresses that had been measured by hydraulic fracturing (see Forbes et al., 2019). The inferred horizontal stresses are shown in Figure 5. Note that the measured horizontal stresses fall into a range, and a "likely" stress value was inferred. The calibrated minimum horizontal stress (from adjusted well logs) matches the DFIT range. Figure 6 shows the full section of log-derived geomechanics data from run 1, below the upper casing.

The stress magnitudes and their variation with depth are also important because they are needed for predicting the vertical and lateral growth of hydraulic fractures as well as their complexity. Hydraulic fracture complexity refers to the degree of branching and interactions with pre-existing natural fractures. The magnitudes of the three principal stresses also govern shearing along pre-existing discontinuities (Zoback, 2012). Reliable vertical profiling of the minimum principal stress allows for numerical simulation of the amount of upwards fracture growth. In an enhanced geothermal system, where an injection well needs to connect with a vertically displaced production well through fracture networks, predictions of the vertical extent of the fractured zone impact the trajectories and separation of the injection and production wells.

LOG-CORE DEPTH ALIGNMENT

The FMI image and the gamma-ray track from run 1 were used with a core gamma-ray measurement to align the two recovered cores to the well logs. The driller's depth (the depth estimated during drilling by tallying drillpipe) for the lower

core was ~14 ft shallower than the equivalent section in the logs (estimated through the amount of wireline extended), and the driller's depth for the upper core was ~11 ft shallower than the equivalent section in the logs (this is possible because of cable stretch in the logging tool wireline). This is shown in Figure 7, where the core gamma-ray and core photos have been shifted to match the FMI and log gamma ray. The core-measured magnetic susceptibility (MS) is also plotted in a shifted position. The alignment of the upper core was based on a prominent igneous dike in the core that was also seen as a prominent sinusoid (the representation of a dipping plane on the unwrapped cylinder of the borehole wall) in the FMI at 6816.5 ft (MD on the log).

Available log data from other wells in the FORGE study area were also compiled. These data were digitized from paper copies and input into the interpretation software (Techlog). A selection of the wells is shown in Appendix 2. The cross section is flattened to the top of crystalline rock, below the alluvium. This boundary is recognizable in the FMI surveys in well 58-32 at ~3176 ft MD. By looking at the other log responses across this boundary in well 58-32 and comparing to those same logs in the other wells (since none had an FMI), we were able to modify the depths of the top of granite across the area. At the time the other wells were drilled, initial depth picks of the top of the granite were made from cuttings collected at the time of drilling and from the decrease in drilling rate, which is much less precise than picking through logs if the top is readily identified through log character.

CONCLUSIONS

Wireline logs are an important tool for characterizing subsurface rock properties in both hydrocarbon and geothermal systems. They provide a wellbore-scale characterization, unlike seismic which samples larger dimensions at a lower resolution. Logs are particularly important in geothermal settings where seismic exploration can be restricted by attenuation and lack of reflectors in the granite and where other measurements such as magnetotelluric and gravity surveys lack resolution. The logging data contain a more diverse set of measurements than seismic data, and at a higher resolution. Additionally, in geothermal systems, seismic imaging is particularly challenging as resolution of features below the basin-fill (in this case) contact is virtually impossible due to the strength of the reflector at the contact and subsequent ray dispersion. The main value of the seismic data at this location is in identifying gross subsurface structures and the depth to the top of the granite. Detection of smaller scale fractures and faults within granitic material is masked by the properties of the granite itself, leaving logs and core as the only viable, high-resolution detection tools, at least for deep granitic systems.

Given the need to hydraulically fracture the FORGE-type, enhanced geothermal systems to set up convective water circulation, geomechanical properties are critical data in addition to fracture detection. Both were obtained in well 58-32 with wireline logging. In addition, fracture system development was resolvable by comparing FMI images before and after the fracture hydraulic injection program.

Fracture identification shows a dominantly NE-SW oriented set of injection- or drilling-induced fractures, suggesting this as the direction of maximum horizontal stress. An orthogonal borehole breakout orientation confirms this. Additionally, after the hydraulic injection, there are numerous zones of increased fracture intensity, such as ~7490–~7505 ft MD and ~7522 –~7535 ft MD, in the section below casing where the FMI was run twice. Image subtraction of the post-fracture FMI from the pre-fracture FMI shows changes in fracture width and extent resulting from hydraulic pressure during the injection program.

Downhole testing, via the DFIT (Forbes et al., 2019), shows a minimum horizontal stress gradient of around 0.62 psi/ft. Log interpretation was able to confirm this individual measurement and estimate the stress gradient variation with depth along the borehole.

ACKNOWLEDGMENTS

Funding for this work was provided by the U.S. DOE under grant DE-EE0007080, "Enhanced Geothermal System Concept Testing and Development at the Milford City, Utah FORGE Site". We thank the many stakeholders who are supporting this project, including Smithfield Foods, Inc., Utah School and Institutional Trust Lands Administration, Beaver County, and the Utah Governor's Office of Energy Development. We would also like to thank Schlumberger for providing logging and interpretation services.

REFERENCES

Crystran, 2018, Quartz sample specification: Online, https://www.crystran.co.uk/optical-materials/quartz-crystal-sio2

Detournay, E., and Cheng A.H.-D., 1993, Chapter 5—Fundamentals of poroelasticity, *in* Fairhurst, C., editor, Comprehensive rock engineering—Principles, practice and projects, volume II—Analysis and design methods: Oxford, Pergamon Press, p. 113–171.

Eaton, B.A., 1969, Fracture gradient prediction and its application in oilfield operations: Journal of Petroleum Technology, v. 246, p. 1353–1360.

Jaeger, J.C., Cook, N.G.W., and Zimmerman, R.W., 2009, Fundamentals of rock mechanics, 4th Edition: Malden, Blackwell Publishing, 488 p.

Krygowski, D.A., 2003, Guide to petrophysical interpretation: Austin, Texas, 147 p.

Schlumberger, 1989, Log interpretation principles/applications: Sugar Land, Schlumberger Wireline and Testing, 241 p.

Ulusay, R., and Hudson, J.A., editors, 2007, The complete ISRM suggested methods for rock characterization, testing and monitoring—1974-2006:ISRM Turkish National Group, Ankara, Turkey, 628 p.

Zoback, M.D., 2012, Reservoir geomechanics, 7th printing: New York, Cambridge University Press, 449 p.